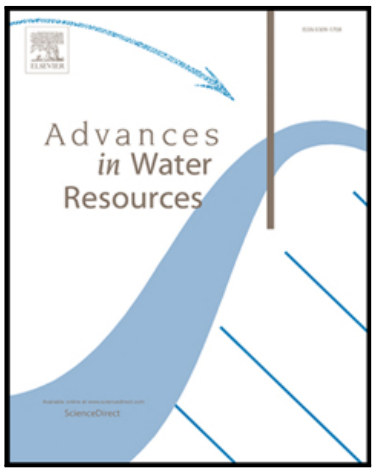

Impacts of secondary and quarter-diurnal tidal species on backwater hydrodynamics in tidal rivers

Min Zhang , Hao Yang , Qibang Tang , Huayang Cai , Zhenchang Zhu , Aichun Feng , Min Luo , Hongkai Gao , Xin Tian

PII: S0309-1708(19)30804-8
DOI: https://doi.org/10.1016/j.advwatres.2020.103660
Reference: ADWR 103660

To appear in: *Advances in Water Resources*

Received date: 7 September 2019
Revised date: 5 May 2020
Accepted date: 13 June 2020

Please cite this article as: Min Zhang , Hao Yang , Qibang Tang , Huayang Cai , Zhenchang Zhu , Aichun Feng , Min Luo , Hongkai Gao , Xin Tian , Impacts of secondary and quarter-diurnal tidal species on backwater hydrodynamics in tidal rivers, *Advances in Water Resources* (2020), doi: https://doi.org/10.1016/j.advwatres.2020.103660

Highlights

- Analytical decomposition of the residual water level slope into river flow, tide-river interaction and tidal asymmetry contributions.
- River flow and tide-river interaction contributions to the residual water level are dominant along the Yangtze estuary.
- Residual water levels caused by tide-river interactions are mainly induced by the semidiurnal tidal species.

Impacts of secondary and quarter-diurnal tidal species on backwater hydrodynamics in tidal rivers

Min Zhang[a], Hao Yang[b,c], Qibang Tang[b,c] , Huayang Cai[b,c*], Zhenchang Zhu[d], Aichun Feng[e], Min Luo[f], Hongkai Gao[g] and Xin Tian[h]

[a]*School of Environmental and Geographical Sciences, Shanghai Normal University, Shanghai, China*

[b]*Institute of Estuarine and Coastal Research/ Guangdong Provincial Engineering Research Center of Coasts, Islands and Reefs, School of Marine Engineering and Technology, Sun Yat-sen University, Guangzhou, China*

[c]*Southern Marine Science and Engineering Guangdong Laboratory (Zhuhai)/ State and Local Joint Engineering Laboratory of Estuarine Hydraulic Technology, Guangzhou, China*

[d]*Institue of environmental and ecological Engineering, Guandong University of Technology, Guangzhou, China*

[e]*Department of Civil and Environmental Engineering, National University of Singapore, Kent Ridge, Singapore*

[f]*Zienkiewicz Centre for Computational Engineering, College of Engineering, Swansea University, Swansea, United Kingdom*

[g]*Key Laboratory of Geographic Information Science (Ministry of Education of China), East China Normal University, Shanghai, China*

[h]*Department of Water Management, Delft University of Technology, Delft, The Netherlands*

Corresponding author: Huayang Cai

Corresponding author's E-mail: caihy7@mail.sysu.edu.cn

Abstract

As river flow debouches into the sea, it is affected by the tidal fluctuation at the estuary mouth, which results in a backwater zone, where the rising residual water level (averaged over a lunar day) in the landward direction is changing periodically. This is known as backwater hydrodynamics,

especially the variation of the residual water levels that are controlled by the interplay between tide and river flows, while these hydrodynamics follow the traditional stage-river discharge relation in the upstream river-dominated region. However, the tidal asymmetry contributions to the residual water level that are caused by secondary tidal species (e.g., diurnal tide D_1), overtide generation (e.g., the quarter-diurnal tide D_4) and their interplay with river flow are poorly understood. In this study, we aim to understand the impacts of secondary and quarter-diurnal tidal species on the increase in residual water level in tidal rivers. To quantify the contributions made by different components, we decomposed the numerically computed subtidal friction into different components representing the contributions made by the river flow alone, the tide-river interaction, and tidal asymmetry due to the nonlinear interaction between different tidal species. The results show that the contribution by tidal asymmetry to the residual water level is minor, while the contributions by river flow and tide-river interaction are dominant, accounting for more than 90% and 80% at the upstream and downstream end of the estuary, respectively. The contribution made by river flow increases, while the tide-river interaction decreases in the landward direction. The semidiurnal tidal species (D_2) predominantly control the residual water level induced by the tide-river interaction along the Yangtze estuary, which accounts for 70%, while the contributions made by the diurnal and quarter-diurnal tidal species are minor and comparable in magnitude in the seaward reach where tide-river interactions are important. The method proposed in this study to quantify the contributions of river flow and different tidal species to the residual water level will enhance our understanding of riverine and tidal impacts on estuarine backwater hydrodynamics and can be used to guide effective and sustainable water management in the Yangtze estuary and other tidal rivers with substantial river flow.

Keywords: residual water level; river flow; tide-river interaction; tidal asymmetry; tidal species

1. Introduction

Rivers connected to the sea can be subject to considerable tidal influence imposed by the coastal ocean. Understanding backwater hydrodynamics in the tide-dominated portions of estuaries (termed here as tidal rivers) are generally essential for coastal flooding, channel navigation, sediment transport, water and ecological management (Munier et al., 2008; Lamb et al.,

2012; Hoitink and Jay, 2016). The increased friction tends to rise the residual water level along the tidal river due to the nonlinear interaction between the tidal flow and river discharge (LeBlond, 1979; Godin and Martínez, 1994; Buschman et al., 2009; Sassi and Hoitink, 2013; Zhou et al., 2018; Kästner et al., 2019). In particular, the residual friction can be cumulative upstream along the tidal river and hence the resulted water level setups impact further inland than the tide-dominated portions (Buschman et al., 2009; Zhang et al., 2018; Kästner et al., 2019).

The occurrence of backwater hydrodynamics is mainly associated with the interaction between the predominant tidal constituent (e.g., M_2 or K_1) and river discharge (Buschman et al., 2009; Sassi and Hoitink, 2013; Kästner et al., 2019). However, the generation of M_4, which is the main source of asymmetry in tidal rivers, is also considered to have an important influence on backwater hydrodynamics in a number of studies (Godin and Martínez, 1994; Cai et al., 2014b; Guo et al., 2015). In addition, the backwater effect can also be produced through the generation of compound overtides (LeBlond, 1979; Buschman et al., 2009). In particular, in the semidiurnal estuary, the interaction of the compound tides MS_4 and $2MS_6$ with river discharge can produce residual water levels, while in the mixed or diurnal estuary where the tidal constituents of O_1 and K_1 are stronger than the M_2 tide, the interaction of the astronomical diurnal tide and river discharge may result in a fortnightly modulation in residual water level variations in the tidally dominated area, which results in a higher residual water level during the spring tide than during the neap tide (LeBlond, 1979; Cai et al., 2018). Conversely, in the river-dominated area, the magnitude of residual water levels is mainly controlled by the variation in river flow (Sassi and Hoitink, 2013; Cai et al., 2018; Zhang et al., 2018).

To understand the interactions between river flow and tidal motion in a tidal river, many researchers decomposed subtidal friction into the different components contributed by tides, rivers and tide-river interactions (Dronkers, 1964; Godin, 1991; Godin, 1999; Buschman et al., 2009; Sassi and Hoitink, 2013). Specifically, Dronkers (1964) adopted the Chebyshev polynomial approach to approximate the nonlinear behavior of bottom friction in a general formula, where the resulting approximation consists of arbitrary number of terms with coefficients that depend on the ratio of river flow velocity to the tidal velocity amplitude. Later, Godin (1991, 1999) proposed a compact approximation to bottom friction that retains only the first and third order terms of the dimensionless velocity, which is comparable with Dronker's formula in terms of accuracy.

Recently, Kästner et al. (2019) revisited the tidal wave propagation along a river with sloping bed and explored how the subtidal water level setups vary with tide-river interaction. Similarly, they decomposed nonlinear quadratic velocity into three terms as a function of the dimensionless velocity.

Alternatively, in order to investigate the effect of non-stationary tide-river interactions, several methods have been proposed, including continuous wavelet transform (e.g., Jay and Flinchem 1997), complex demodulation (e.g., Jay and Kukulka 2003), short-term harmonic analysis (e.g., Guo et al. 2015), nonstationary tidal analysis (e.g., Matte et al. 2013, 2014), and enhanced harmonic analysis (e.g., Pan et al. 2018). These methods together with analytical decomposition methods (e.g., Dronkers, 1964) are helpful for quantifying the relative importance of river flow, tide-river interactions and tidal flow on the residual water level by means of decomposing the subtidal friction, which is mainly balanced by the residual water level slope; however, the contributions made by secondary tidal species (e.g., diurnal tide D_1) and quarter-diurnal overtide (e.g., D_4) to the generation of residual water level (and hence backwater hydrodynamics) are not yet fully understood.

Recently, Cai et al. (2014a, 2014b, 2016) proposed an analytical approach to determining backwater hydrodynamics in tidal rivers. However, the theoretical analysis only accounts for one predominant tidal constituent (e.g., semidiurnal M_2 tide), while the major secondary tidal species (e.g., D_1) and the contribution made by tidal asymmetry due to overtide generation (e.g., D_4) and their interplay with river flow are poorly understood. In this paper, a fully nonlinear 2D numerical model is used to help understanding the impacts of the secondary tidal species and a nonlinear D_4 overtide on backwater hydrodynamics. The key objective is the decomposition of the quadratic velocity in the friction term, which allows for the quantification of different components (i.e., tide, river and tide-river interaction) of the residual water level. Then, the relative importance of each contribution is explored.

Understanding the causes of residual water level setups are important for interpreting the influences of backwater hydrodynamics, which may provide new insights into how the primary tidal species and tide-river interactions physically influence the morphology, hydrology and ecology in estuaries. Zhang et al. (2018) suggests that tide-river interactions influence tidal asymmetry by modulating residual water levels and are a key factor controlling sediment transport

and hence the morphodynamics. Hoitink and Jay (2016) have emphasized the special vulnerability of deltas to mean sea level rise by focusing on the additional effect of water level setup from nonlinear interaction between river discharge and the tides, which will not only exacerbate problems of flood vulnerability but also limit freshwater availability due to enhanced salinity intrusion. Sassi and Hoitink (2013) argued that the location where the amplitude of seasonal residual water level variation is comparable to that of the primary tidal constituent indicates a transition between tidal and fluvial dominance. This location is around Zhenjiang to Jiangyin in the Yangtze estuary, where the flow ceases to reverse in direction during the dry and wet seasons, respectively (Guo et al., 2015). In this transitional zone, the seasonal variation of the flow reversal and backwater hydrodynamics affects channel morphology and riparian ecology in terms of inundation frequency, flow velocity and sediment transport.

The remainder of the paper is arranged as follows. In the following section, the analytical description of the residual water level slope and decomposition method of the subtidal friction into contributions by river flow alone, tide-river interaction and tidal asymmetry components are introduced. Subsequently, the analytical decomposition method is applied to the Yangtze estuary, where the velocity and water level fields are extracted by using a numerical model (section 3). In this section, the decomposition of the tide into its main constituents and the decomposition of the residual water level slope into different contributions made by rivers, tide-river interactions and tides are presented. In section 4, the relative importance of various tidal species, the channel convergence (i.e., landward decrease in cross-sectional area) role on the backwater hydrodynamics, some other factors that can influence the subtidal water level offset, and the implications for tidal rivers are discussed. Finally, the conclusions are presented in section 5.

2. Methodology

The key for quantifying the impacts of secondary and quarter-diurnal tidal species on backwater hydrodynamics lies in the decomposition of the residual water level slope into different contributions made by rivers, tide-river interactions and tides, where the last two components depend on wave behavior of different tidal species. It is well known that the residual water level slope is primarily balanced by the residual frictional effect (e.g., Buschman et al., 2009; Sassi and Hoitink, 2013, see a brief derivation in Section 2.1), which is a quadratic function of the velocity. Hence, a linearization of the squared velocity is required in order to link the residual water level

slope to the contributions made by different tidal species (see Section 2.2). Subsequently, the impact of individual tidal species on the backwater hydrodynamics can be quantified based on the harmonic constants (i.e., amplitude and phase) derived either from observed or numerically computed time series of velocity. In this study, a schematized numerical model with a simplified estuarine geometry was adopted to obtain the required velocity fields (see Section 2.3). Note that we mainly focus on the residual water level dynamics relative to the mean water level at the estuary mouth, therefore the influence of seasonal variation of mean sea level over a year is implicitly taken into consideration when subtracting the mean water level at the estuary mouth for the residual water level along the channel.

2.1 An analytical decomposition of the residual water level slope

The residual water level slope can be determined from the simplified 1D momentum equation when the density stratification and internal waves are negligible, which is described as follows:

$$\frac{\partial U}{\partial t} + U\frac{\partial U}{\partial x} + g\frac{\partial Z}{\partial x} + g\frac{U|U|}{K^2 h^{4/3}} = 0, \tag{1}$$

where U is the cross-sectional average velocity, Z is the free surface elevation, h is the water depth, g is the gravity acceleration, t is the time, x is the longitudinal coordinate directed landward, and K is the Manning-Strickler friction coefficient.

Assuming a periodic variation in flow velocity, the integration of Eq. (1) over a tidal cycle leads to the following expression (Vignoli et al., 2003; Cai et al., 2014b):

$$\frac{\partial \overline{Z}}{\partial x} = -\frac{1}{K^2}\overline{\left(\frac{U|U|}{h^{4/3}}\right)} - \frac{1}{2g}\frac{\partial \overline{U^2}}{\partial x}. \tag{2}$$

where the overbars denote the tidal average. The second contribution in Eq. (2) to the residual water level originates from the advective acceleration, which is relatively small when compared to the first contribution induced by the residual frictional effect as long as the Froude number is small.

2.2 Analytical decomposition of the residual water level slope

It was shown by Hoitink et al. (2003) that tidal constituents with similar angular frequency can be lumped into a single combined harmonic. Thus, for the case in a tidal river considering 3 principle tidal species, i.e., diurnal tidal species (D_1), semidiurnal tidal species (D_2) and quarter-diurnal species (D_4), extracted using the Fourier analysis, the cross-sectional flow velocity U at a specific position can be approximated by the following expression:

$$U(t) = -u_0 + \upsilon_1 \cos(\omega t + \psi_1) + \upsilon_2 \cos(2\omega t + \psi_2) + \upsilon_4 \cos(4\omega t + \psi_4), \tag{3}$$

where t is time, u_0 is the residual flow velocity mainly generated by the river flow, υ_1, υ_2 and υ_4 are the velocity amplitudes of D_1, D_2 and D_4, respectively, ω is the frequency of the diurnal tide and ψ_1, ψ_2 and ψ_4 are the velocity phases of D_1, D_2 and D_4, respectively. Godin (1991, 1999) showed that the quadratic velocity $U|U|$ in the momentum equation can be approximated by the Chebyshev polynomials approach, which leads to the following equation:

$$U|U| = \upsilon'^2 \left\{ \begin{array}{l} \frac{16}{15\pi}\left[-\varepsilon_0 + \varepsilon_1 \cos(\omega t + \psi_1) + \varepsilon_2 \cos(2\omega t + \psi_2) + \varepsilon_4 \cos(4\omega t + \psi_4)\right] + \\ \frac{32}{15\pi}\left[-\varepsilon_0 + \varepsilon_1 \cos(\omega t + \psi_1) + \varepsilon_2 \cos(2\omega t + \psi_2) + \varepsilon_4 \cos(4\omega t + \psi_4)\right]^3 \end{array} \right\}, \tag{4}$$

where υ' is the maximum possible value of the velocity (i.e., $\upsilon' = u_0 + \upsilon_1 + \upsilon_2 + \upsilon_4$), and $\varepsilon_0 = u_0/\upsilon'$, $\varepsilon_1 = \upsilon_1/\upsilon'$, $\varepsilon_2 = \upsilon_2/\upsilon'$ and $\varepsilon_4 = \upsilon_4/\upsilon'$ are the dimensionless velocity amplitudes scaled by the maximum velocity υ'.

Making use of the trigonometric equations to expand the power of the cosine functions (e.g., $\cos^3(\omega t + \psi_1)$ and $\cos^2(\omega t + \psi_1)$) and extracting the original harmonics with frequencies of ω, 2ω and 4ω, Eq. (4) can be reduced as follows:

$$U|U| = \upsilon'^2\left[F_0 + F_1 \cos(\omega t + \psi_1) + F_2 \cos(2\omega t + \psi_2) + F_4 \cos(4\omega t + \psi_4)\right], \tag{5}$$

with

$$F_0 = -\frac{16}{15\pi}\varepsilon_0\left[1 + 2\varepsilon_0^2 + 3\varepsilon_1^2 + 3\varepsilon_2^2 + 3\varepsilon_4^2 - \frac{3}{2}\frac{\varepsilon_1^2\varepsilon_4}{\varepsilon_0}\cos(\psi_4 - 2\psi_1) - \frac{3}{2}\frac{\varepsilon_2^2\varepsilon_4}{\varepsilon_0}\cos(\psi_4 - 2\psi_2)\right], \tag{6}$$

$$F_1 = \frac{16}{15\pi}\varepsilon_1\left(1 + 6\varepsilon_0^2 + \frac{3}{2}\varepsilon_1^2 + 3\varepsilon_2^2 + 3\varepsilon_4^2\right), \tag{7}$$

$$F_2 = \frac{16}{15\pi}\varepsilon_2\left(1 + 6\varepsilon_0^2 + 3\varepsilon_1^2 + \frac{3}{2}\varepsilon_2^2 + 3\varepsilon_4^2\right), \tag{8}$$

$$F_4 = \frac{16}{15\pi}\varepsilon_4\left(1 + 6\varepsilon_0^2 + 3\varepsilon_1^2 + 3\varepsilon_2^2 + \frac{3}{2}\varepsilon_4^2\right). \tag{9}$$

For illustration, approximations using Eqs. (4) and (5) with $\varepsilon_0 = 0.3$, $\varepsilon_1 = 0.1$, $\varepsilon_2 = 0.05$, and $\varepsilon_4 = 0.4$ are displayed in Fig. 1. The Chebyshev polynomial approximation (4) matches the nonlinear quadratic velocity well, while Eq. (5), which retains only the original frequencies (ω, 2ω and 4ω), approximately captures the first-order trend of the quadratic velocity.

Hence, it follows directly from Eqs. (2) and (5) that the residual water level slope is given as follows

$$\overline{\frac{\partial Z}{\partial x}} = -\frac{\upsilon'^2}{K^2\overline{h^{4/3}}}F_0 = \underbrace{\frac{\upsilon'^2}{K^2\overline{h^{4/3}}}\left[\frac{16}{15\pi}\varepsilon_0\left(1+2\varepsilon_0^2\right)\right]}_{f_r} + \underbrace{\frac{\upsilon'^2}{K^2\overline{h^{4/3}}}\left[\frac{16}{15\pi}\varepsilon_0\left(3\varepsilon_1^2+3\varepsilon_2^2+3\varepsilon_4^2\right)\right]}_{f_{tr}} - \underbrace{\frac{\upsilon'^2}{K^2\overline{h^{4/3}}}\left\{\frac{16}{15\pi}\left[\frac{3}{2}\varepsilon_1^2\varepsilon_4\cos\left(\psi_4-2\psi_1\right)+\frac{3}{2}\varepsilon_2^2\varepsilon_4\cos\left(\psi_4-2\psi_2\right)\right]\right\}}_{f_t} \tag{10}$$

where the terms f_r, f_{tr} and f_t quantify the river flow alone, tide-river interaction and tidal asymmetry contributions to the resulting residual water level relative to the mean water level at the estuary mouth, respectively. Note that the contribution of tidal asymmetry f_t depends on the relative phase difference among diurnal, semidiurnal and quarter-diurnal species, thus the Fourier analysis is required in order to derive the harmonic constants (including tidal velocity amplitudes and phases) for different tidal species as the inputs for Eq. (10).

In Eq. (10), it should be noted that we implicitly assumed that $\overline{\frac{1}{h^{4/3}}} = \frac{1}{\overline{h}^{4/3}}$, i.e., neglecting the non-linearity of the periodic variation of water depth in the denominator of the friction term. This is not a restrictive assumption as long as the tidal amplitude to the depth ratio is small, which is generally the case in alluvial estuaries (e.g., Savenije, 2012). However, this non-linearity on the residual water level setup would become important since it is the main underlying mechanism that draws the water surface back to the level that it would without tides far upstream from the sea (Kästner et al., 2019). In this study, we mainly concentrate on backwater hydrodynamics in the downstream part of the estuary so that we ignore the influence of non-linearity of the periodic variation of water depth on residual water level setup.

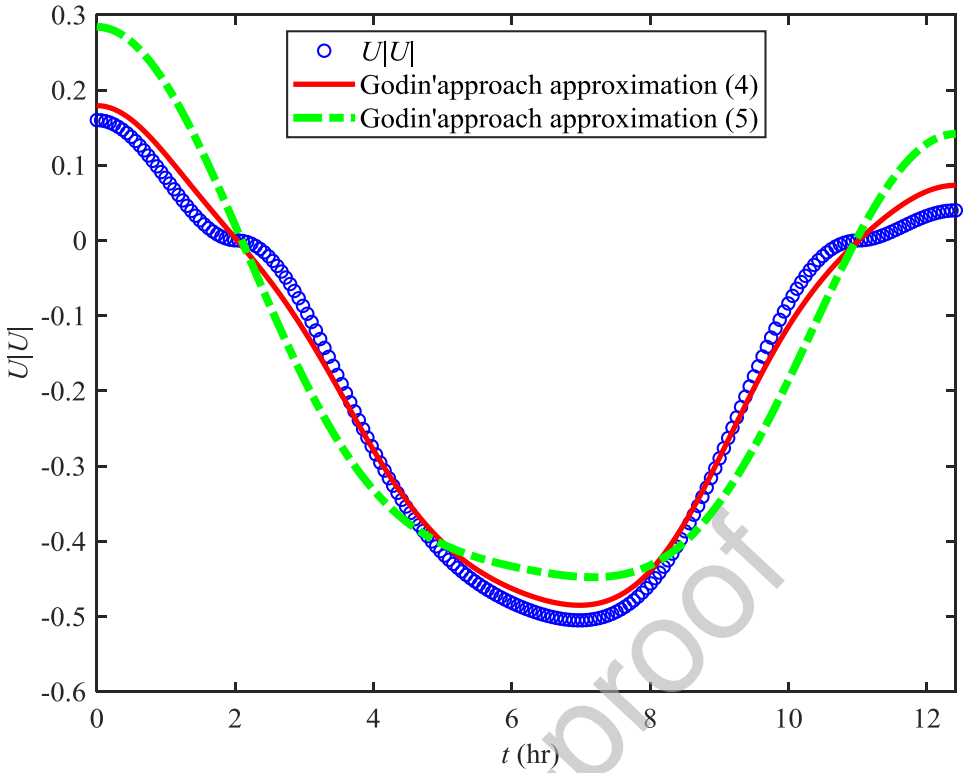

Fig. 1. Approximation of the quadratic velocity $U|U|$ by the Chebyshev polynomials approach for the case of three tidal constituents. Here, $U = -0.3 + 0.1\cos(\omega t) + 0.05\cos(\omega t) + 0.4\cos(2\omega t) + 0.1\cos(2\omega t) + 0.05\cos(4\omega t)$, where ω represents the tidal frequency of the diurnal component.

2.3 Numerical description of a schematized tidal river model

Since the existing analytical model (e.g., Cai et al., 2014a, 2014b, 2016, 2019) is only able to reproduce the backwater hydrodynamics accounting for one predominant tidal constituent (e.g., semidiurnal M_2 tide), a schematized numerical model is used to help understanding the backwater hydrodynamics accounting for various tidal constituents. In particular, the numerical model provides high-resolution velocity fields that can be used to decompose into different tidal species for further analysis by means of the analytical decomposition method presented in Section 2.2. The numerical model is constructed using the unstructured finite element model TELEMAC-2D, which solves the Navier-Stokes equations for an incompressible fluid under shallow water and the Boussinesq assumptions. The controlling equations were discretized and solved based on irregular triangular meshes, which were suitable for representing the curved riverbanks and irregular shorelines of a natural estuary. For more details on the governing equations, the reader is referred to Hervouet (2000) and the TELEMAC-2D user's manual (Operating Manual, 2016). To better

represent the geometry of the tidal river with funnelling width and prismatic cross section, model channel width B and cross-sectional area A were generated based on the following expressions on a tidally averaged scale (Cai et al., 2014a; Toffolon et al., 2006):

$$B = B_r + (B_0 - B_r)\exp\left(-\frac{x}{b}\right), \tag{11}$$

$$A = A_r + (A_0 - A_r)\exp\left(-\frac{x}{a}\right), \tag{12}$$

where B_0 and B_r represent the channel width at the seaward end and landward end, respectively, A_0 and A_r represent the cross-sectional area (below the mean sea level) at the seaward end and landward end, respectively, and a and b are the convergence lengths of cross-sectional area and channel width, respectively.

The above Eqs. (11)-(12) account for not only the exponential convergence estuary in the seaward part but also the constant width and cross-sectional area in the landward part. Figure 2a shows the model geometry used in this study. By changing the convergence length b, the geometry shows no inflection point of the transition from exponential river mouth to constant river channel. Assuming that the cross section of the estuary is schematized as rectangular, the bathymetric depth is given by $H = A/B$, and is defined as the bed elevation z_b relative to a fixed datum (Fig. 2b). The hydraulic depth is different from the distance between mean sea level and bed level, and is defined as the tidally averaged depth h between the mean water level z_{ws} and the bed level z_b (see Fig. 2b).

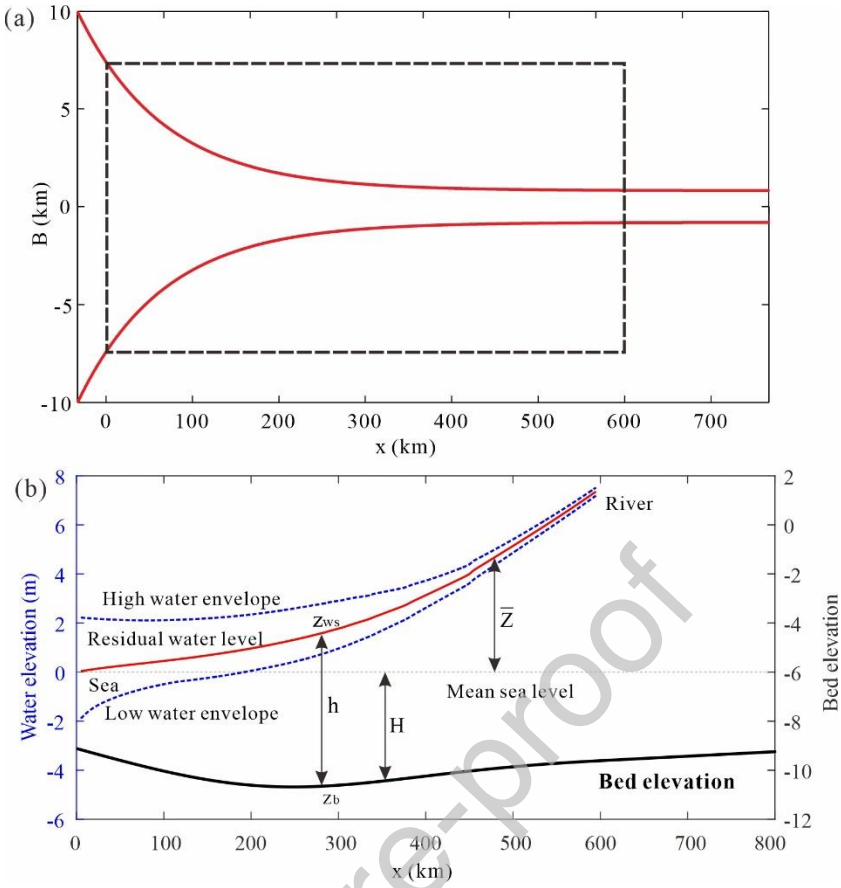

Fig. 2. Geometry of the schematized tidal river (presented in a distorted length scale) for (a) channel width and (b) water levels together with the bed elevation.

3. Application to the Yangtze estuary

3.1 Physical setting of the Yangtze estuary

The Yangtze River is the third longest and the fourth largest river in the world in terms of freshwater discharge, and the river stretches approximately 6,300 km from the Tibetan Plateau in the west to the East China Sea near Shanghai. The Yangtze River drains a catchment of approximately 1.8 million km^2 and has a strongly seasonal variation in flow rate (Xu and Milliman, 2009). Estuarine studies typically focus on the reach downstream of Datongzhen (in Anhui province) (Fig. 3a), where there is a hydrological station (i.e., Datong) that indicates the influence of tidal flow is vanishing (Zhang et al., 2016a). This reach is approximately 600 km long and flows through a flat alluvial plain, where the valley gradient is small and the river meanders extensively. The main course of the river is constrained at intervals by bedrock that gives rise to narrow gorges followed by pools and islands, causing the channel to branch (Fig. 3a). Tidal effects become considerable downstream of the large bend approximately 250 km from the mouth and are

dominant over the last 150-200 km (Zhang et al., 2016a), resulting in a well-defined branching structure. The South Branch is the main channel outlet conveying more than 98% of the river flow, while the North Branch is connected perpendicular to the South Branch and functions in isolation (Dai et al., 2016) (see their positions in Fig. 3a). Therefore, we only consider the South Branch and the river channels further upstream until the Datong hydrological station in the following analysis.

The tides are semidiurnal with a meso-tidal range in the South Branch, near the mouth, varying from 1 to 4 m over the spring-neap cycle (Wu et al., 2012). There exists a strong tidal asymmetry; thus, the flood tide lasts approximately for 5 hours during spring tides, whereas the ebb tide lasts for approximately 7.5 hours (Zhang et al., 2016a). The river discharge is highly variable on a seasonal time-scale. Data used at Datong (1956-2009) suggest that the average freshwater discharge is approximately 20,000 m^3 s^{-1}, with the monthly mean varying between 7,600 m^3 s^{-1} in February 1987 and 66,200 m^3 s^{-1} in July 1983. As a result, the Canter-Cremers number, indicating the ratio of freshwater discharge to saline water entering the estuary over a tidal cycle, varies significantly between ~0.1 for the dry season and ~0.5 for the wet season. Such a strong variation in the Canter-Cremers number indicates that the South Branch of the estuary is a well-mixed channel during the dry season but becomes more stratified during the wet season, especially during the neap tides. In this study, we mainly focus on the dominant tide-river interaction process in the Yangtze estuary; hence, the influence of the sediment flux dynamics on the tide-river interaction is neglected.

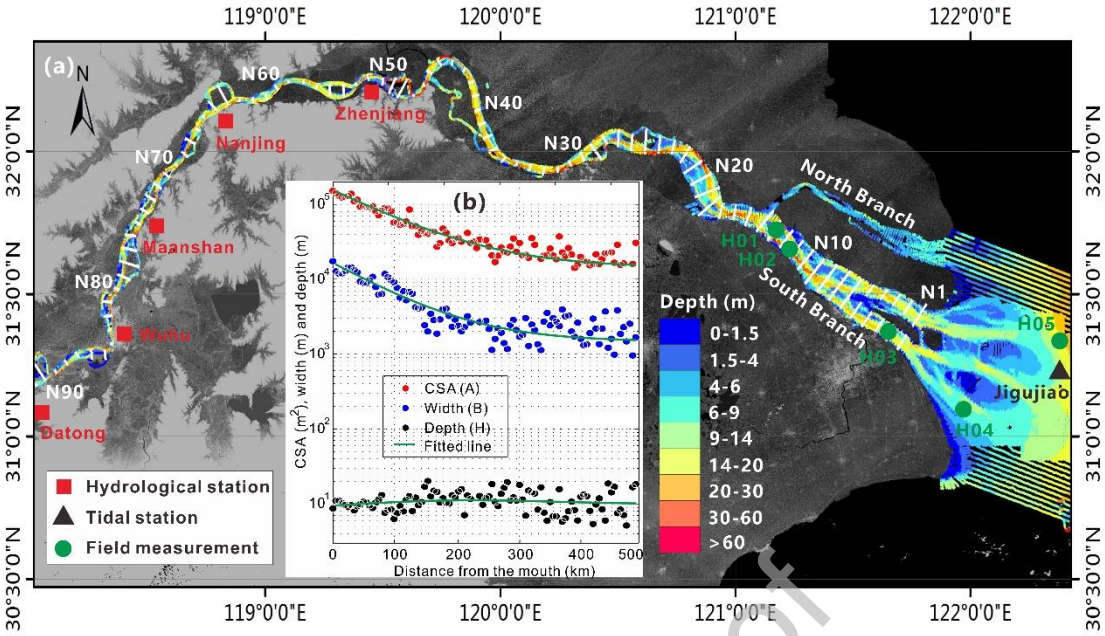

Fig. 3. Map of the Yangtze estuary: (a) the field measuring point and location of cross-sections, (b) the geometric parameters of the cross-sectional area (CSA) *A*, width *B*, and depth *H* along the Yangtze estuary. The green lines represent the best-fitting curves.

3.2 Description of the geometric boundary

To quantify the secondary and quarter-diurnal tidal species on the backwater hydrodynamics, a schematized numerical model reproducing the main tide-river dynamics in the Yangtze estuary was constructed, with the domain width converging from the mouth to 600 km at the upstream boundary. The length of the model domain is extended from approximately -50 km at the offshore area to 800 km in the upstream boundary to avoid boundary effect. An unstructured triangular mesh was generated, with a low-resolution seaward (average cell size of 7000 m) and relatively high resolution (average cell size of 300 m) landward. Navigational charts of 2007 and 2008 covering the entire Yangtze estuary were used to define the estuary and river channel elevations (Fig. 3a). All the depth points were first corrected relative to the national Huanghai 1985 datum and then projected from the WGS-84 geographic coordinates to the UTM-51 coordinates. Figure 3b shows the schematic geometry used in the model, with channel width and cross section area (CSA) converging exponentially from the mouth towards a constant cross section in the river part. The bathymetric depth defined by $H = A/B$ was shown to be maintained at approximately 10 m for the entire estuarine area, with a low bed slope of only ~1:100,000. The positions of the sampling locations are shown as white line segments in Fig. 3a. The present settings of the model geometry

and bathymetry allow nearly complete tidal decay and avoid tidal wave reflection at both the seaward and landward ends.

Similar to the numerical model, the fitted geometry parameters used in the decomposition method presented in Section 2.2 were obtained by fitting Eqs. (11) and (12) against the observed geometric parameters, as shown in Table 1. Conventionally, an exponential function and a linear function were used to fit the geometry by subdividing the Yangtze estuary into two reaches, with an inflection point beyond approximately 280 km where the estuary geometry switches from an exponentially shaped mouth to a prismatic river channel (Cai et al., 2014b; Zhang et al., 2016a). The advantage of the present method is that it describes the whole estuary with a simple expression. The result shows a high correlation coefficient R^2 of 0.97 for the cross-sectional area and 0.94 for the width. Notably, the bathymetric depth H presented in Fig. 2b is the flow averaged depth relative to the Huanghai 1985 datum.

Table 1. The geometrical parameters of the Yangtze estuary.

Geometrical parameter	Mouth (A_0 or B_0)	River (A_r or B_r)	Convergence length (a or b)	R^2
CSA (A), m^2	150,000	14,000	120,000	0.97
Width (B), m	17,000	1,500	100,000	0.94

3.3 Model performance

The computational domain covers the entire Yangtze estuary area, the configuration is shown in Fig. 2. The external forcing considered in the model includes free surface elevations at the seaward boundary and a river discharge imposed at the landward end. Density-effects are neglected in this study, since their effects on the backwater hydrodynamics are rather small compared to the frictional dissipation induced by tide and river discharges (Cai et al., 2016). Hence, the flow is simulated in depth-averaged model.

To demonstrate the capability of the schematized numerical model, the velocities and free surfaces of hydrodynamic model are well verified through the calibration of friction coefficient using the data observed along the Yangtze estuary. In the model calibration, the depth-averaged velocities are obtained in the South Branch and the mouth bar area (see their positions in Fig. 3a). A direct comparison between velocities from the numerical model at the 10 gauging stations

during 22–24 July 2007 (representing a neap tide) and during 29–31 July 2007 (representing a spring tide) is shown in Fig. S1 in the Supporting Information. It can be seen that the reproduced velocities follow the observations satisfactorily, with a coefficient of determination (R^2) of 0.95, although the flow velocity during spring is a little underestimated at some stations and some disagreements occur during the maximum ebb flow. The other parameters used in the numerical model include: a time step of 30 s, a horizontal diffusion viscosity coefficient of 0.1. The bottom friction is prescribed by a decreasing Manning-Strickler friction coefficient along the channel, i.e., a linear reduction from 63 $m^{1/3}$ s^{-1} at the estuary mouth to 37 $m^{1/3}$ s^{-1} at the Datong hydrological station. For detailed descriptions of the model's configuration, readers can refer to other publications, such as Zhang et al. (2016a, b).

A further validation of water levels recorded during 1-30 November 2007 (representing dry season) and during 1-30 September 2007 (representing wet season), is shown in Table S1 in the Supporting Information, which illustrates the comparison between the numerically computed and observed residual water levels (daily averaged) at the 5 gauging stations of Datong, Wuhu, Maanshan, Nanjing and Zhenjiang (see their positions in Fig. 3a) along the Yangtze estuary. These data are corrected and referenced to the Huanghai 1985 datum. The model starts with an initial condition of zero elevation and a simulation period of 37 days, with the first 7 days are considered to be the spin-up period. After 37 days of simulation, the water level data of the last 30 days with an output interval of 15 minutes (same as the computational time step) are averaged to generate the daily mean water level (i.e., the residual water level). Subsequently, the daily mean water levels derived from the numerical model are compared with the field observations in Fig. 4. Overall the computed residual water levels agree well with observations, suggesting that the schematized numerical model reproduces the main tidal-river dynamics in the Yangtze estuary. The scatter reflects the complexity of the real bathymetry, which is substantially simplified for adoption in the numerical model. The presence of many islands and narrow and deep gorges makes the exponentially convergent geometry irregular and fluctuate in the cross-sections. Rapid changes make schematized modeling particularly challenging, and more detailed modeling with real bathymetry is needed if changes over local scales are the focus of interest. However, for this study, the primary interest is in the interactions of the tide and river at an estuarine scale; thus, it is

sufficient to provide information on the relative contributions of different components for the analytical model.

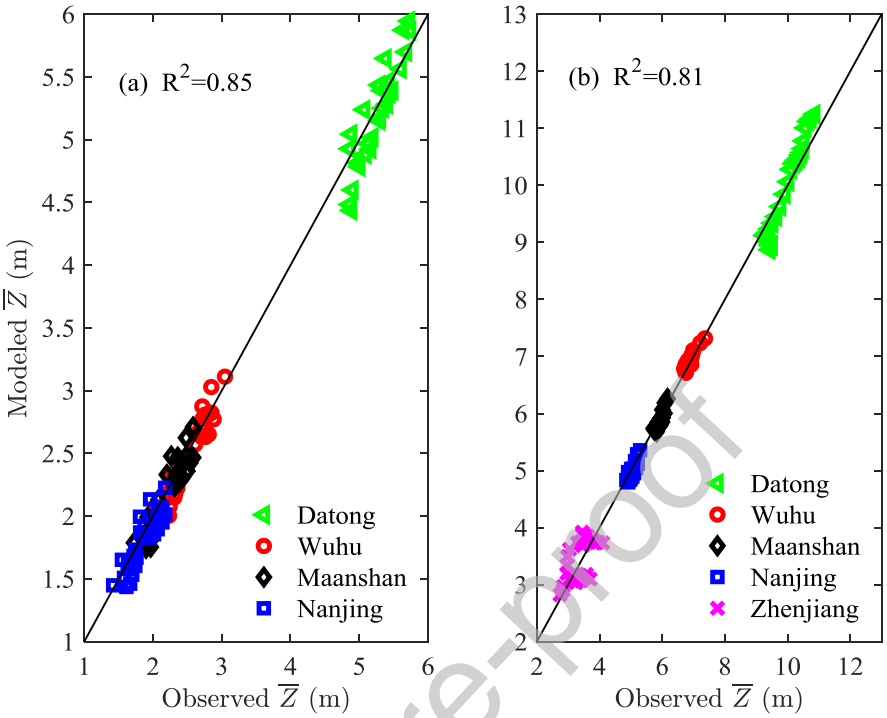

Fig. 4. Comparison of the residual water level between the numerical results and observations in the Yangtze estuary during 1-30 November 2007, representing the dry season (a), and 1-30 September 2007, representing the wet season (b).

3.4 Settings of the numerical experiments and application of the analytical decomposition method to the numerical results

In the current study, we consider the diurnal tide (i.e., K_1 and O_1), semidiurnal tides (i.e., M_2 and S_2) and other secondary astronomical tides imposed at the seaward boundary of the Yangtze estuary. Four sets of numerical experiments were designed to examine the contributions of river discharge, major astronomical tidal species (i.e., D_1 and D_2) and generated quarter-diurnal tide (i.e., D_4) on the backwater hydrodynamics. The amplitudes and phases of 31 tidal components, extracted from long-term free surface fluctuations by means of Fourier analysis of the TPXO7.2 database (www.tpxo.net/global, accessed on 21 April 2020) for typical spring-neap cycles around the Jigujiao Station (see its location in Fig. 3), remain unchanged in all experiments, while that of the river discharge varies in each experiment. River discharges were modelled by four different constant discharges of Q_1=60,000, Q_2=35,000, Q_3=15,000 and Q_4=1,000 m^3/s, representing the

peak (with the return period of approximately 2.5 years), typical wet, typical dry and extremely low runoff (denoted by elr, with the return period of approximately 150 years) conditions in the Yangtze estuary. As a result, the calculated Canter-Cremers numbers at the estuary mouth are approximately 0.92, 0.52, 0.19 and 0.01 for four given river discharge conditions, respectively. The Fourier analysis was carried out at each grid point to derive information on the harmonic constants for the tidal species of diurnal (D_1), semidiurnal (D_2) and quarter-diurnal (D_4) tides of the velocity fields. Subsequently, the extracted tidal current harmonics were used as inputs for the analytical decomposition described in section 2.2, quantifying the contributions made by the river flow alone, tide-river interaction, and tidal asymmetry (due to the phase differences in D_1-D_2 and D_2-D_4). Figure 5 shows a comparison of the residual water level between the fully nonlinear numerically computed results and simplified analytically computed results under four river discharge conditions. The results show highly consistent residual water levels (R^2>0.99 for elr, typical dry season, typical wet season and peak discharge conditions, respectively), demonstrating the good performance of analytical reconstruction approach for the residual water levels described in Eq. (10).

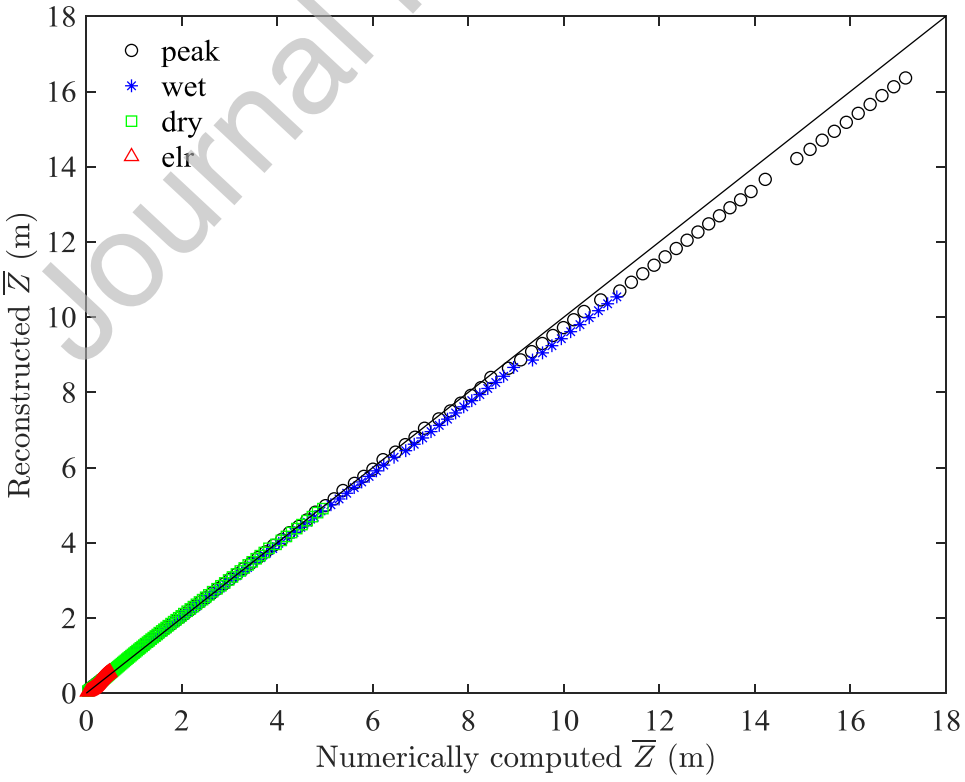

Fig. 5. Comparison of the residual water level between the fully nonlinear numerically computed

results (by TELEMAC-2D) and analytically reconstructed results (only accounting for D_1, D_2 and the overtide D_4 based on the harmonic results from numerical simulations) in the Yangtze estuary for elr, typical dry season, typical wet season and peak discharge conditions.

3.5 The variation of spring-neap change on backwater hydrodynamics

To highlight the importance of spring-neap change on backwater hydrodynamics, the whole time series of tidal variation in 2007 are divided into separate spring and neap periods based on a moving window analysis (see Fig. S2 in the Supporting Information). The 25 hr moving average filter captures the spring-neap cycle very well, which shows an apparent 14.8 d cycle by using the spectral analysis (Fig. S3). The Fourier analysis is then used to extract the tidal properties (including the tidal amplitude and phase) for each sub-period of the spring and neap time series. Longitudinal variations of the residual water level and its slope for the spring and neap periods were then reconstructed by means of the analytical decomposition method presented in Section 2.2 for different river discharge conditions. The comparison between the observed residual water levels and analytically reconstructed values for the mean spring and neap tide periods and for the whole year period are shown in Fig. S4. The performance of the analytical method for reconstructing the residual water level in terms of root mean squared error (RMSE) shows a reasonable accuracy ranging between 0.06 and 0.29 m (Table 2).

The spatially averaged contributions over spring and neap tide made by different forcing components (f_r, f_{tr} and f_t) to the total residual water level, and made by different tidal species (D_1, D_2 and D_4) to the residual water level owing to the tide-river interaction ($\overline{Z_{tr}}$) are shown in Table 3. Overall, the spring-neap change of the contributions made to the residual water levels by diurnal (D_1), semidiurnal (D_2) and quarter-diurnal (D_4) tidal species is relatively minor (<9%) for given imposed constant river discharges at the landward boundary. In addition, the spring-neap change of the contributions made by river flow alone (f_r), tide-river interaction (f_{tr}) and tidal asymmetry (f_t) to the total residual water level is also minor for both the typical wet and dry river discharge conditions (<7%), although the spring-neap change is relatively large for the elr condition (< 53%), which is actually a rare condition occurred approximately once in 150 years. Consequently, due to the fact that the influence of spring-neap change on residual water levels is relatively minor, in the following sections we shall concentrate on the yearly averaged case, but present the cases for the spring and neap tides in the Supporting Information (see Figs. S5-S8).

Table 2. Spatially averaged contributions made from different forcing components (river flow alone f_r, tide-river interaction f_{tr} and tidal asymmetry f_t) and different tidal species (diurnal D_1, semidiurnal D_2 and quarter-diurnal D_4) to the residual water level and to the residual water level owing to the tide-river interaction $\overline{Z_{tr}}$, respectively, for the mean spring, neap tides, and for the whole year periods under elr, dry, wet, and peak river discharge conditions. The RMSE represents the accuracy between the observed residual water level and the analytically reconstructed values.

	Elr			Dry			Wet			Peak		
	Spring	Neap	Year	Spring	Neap	Year	Spring	Neap	Year	Spring	Neap	Year
f_r	51%	32%	41%	69%	69%	71%	80%	81%	83%	86%	88%	89%
f_{tr}	87%	53%	70%	37%	30%	30%	23%	19%	18%	16%	12%	11%
f_t	-37%	16%	-11%	-4%	3%	-1%	-1%	1%	-1%	-1%	0%	0%
D_1	12%	16%	15%	21%	28%	23%	27%	34%	28%	31%	36%	31%
D_2	67%	69%	68%	54%	56%	56%	50%	51%	52%	48%	49%	51%
D_4	21%	15%	17%	25%	16%	21%	23%	15%	20%	21%	15%	18%
RMSE (m)	0.19	0.06	0.15	0.29	0.16	0.23	0.27	0.27	0.28	0.24	0.28	0.28

3.6 Longitudinal variations in the tidal amplitude and phase under different river discharge conditions

Considering the impacts of the seasonal river discharges on the tidal variations, a Fourier analysis procedure executed by the MATLAB program was applied to extract the harmonic constants of the velocity time series for four river discharge cases representing elr, typical dry season, typical wet season and peak discharge conditions. Figures 7-8 illustrate the longitudinal variations of the tidal velocity amplitude and current phases, which include two major astronomical tidal species (D_1 and D_2) and a quarter-diurnal shallow water overtide (D_4). The dominant semidiurnal tidal species D_2 has mean amplitude of approximately 0.6 m/s near the mouth, while the diurnal tidal species D_1 has a mean amplitude of only 0.12 m/s near the mouth, and the amplitude of the quarter-diurnal tidal species D_4 is less than 0.05 m/s near the mouth. To highlight the admittance between different tidal species, the longitudinal variation in the tidal velocity amplitude normalized by the amplitude at the estuary mouth for D_1, D_2 and D_4 under different river discharge conditions are shown in Fig. S9 (see the Supporting Information).

As the tide propagates upstream along the Yangtze estuary, the velocity is generally attenuated due to frictional dissipation (Dalrymple et al., 1992; Dalrymple and Choi, 2007). We

observe an exponential decrease in the D_1 and D_2 amplitudes in the landward direction, while the amplitude of the D_4 overtide reaches a maximum at approximately 150 km before vanishing. In the seaward reach (0-150 km) of the Yangtze estuary, a rapid decrease in the amplitudes of the astronomical tides (D_1 and D_2) and growth of the overtide (D_4) are identified. The evolution of tidal hydrodynamics in estuaries is primarily determined by a combination of frictional dissipation and amplification by channel convergence (Savenije et al., 2008). As noted by Dalrymple et al. (1992) and Dalrymple and Choi (2007), in the "hypersynchronous" system, the effect of channel convergence is stronger than the frictional effect so that the tidal amplitude increases before vanishing. The overtide D_4 had a variable amplitude that differs from the astronomical tides of D_1 and D_2. This phenomenon indicates that the energy of the astronomical tides is transferred to that of the overtide due to the nonlinear dynamics of the shallow water flow, as discussed by Parker (1991), including both the advective acceleration and depth-dependent frictional effect.

Approximately 150 km upstream of the Yangtze estuary, all tidal species D_1, D_2 and D_4 are attenuated nearly monotonically. The continuous damping of the tidal wave indicates that frictional dissipation is the dominant factor in the upstream part of the estuary. In addition, we observe that the larger the imposed river discharge, the greater the damping of the landward tidal amplitude, which is mainly due to the suppression effect of tidal propagation by the increased river discharges. With respect to phases, our results show that the phases of all three major tidal species show a clear increase with the tidal propagation upstream (Fig. 7). The values of the quarter-diurnal tide D_4 clearly vary with the semidiurnal tide D_2, with a relative phase difference ($2\varphi_2 - \varphi_4$) increasing linearly in the landward direction by a slope of approximately 0.8°/km. In all four river discharge conditions, high and low water timings are distorted, but the phases remain nearly unaffected by the river discharge, except for the upstream part during periods of low flow (elr).

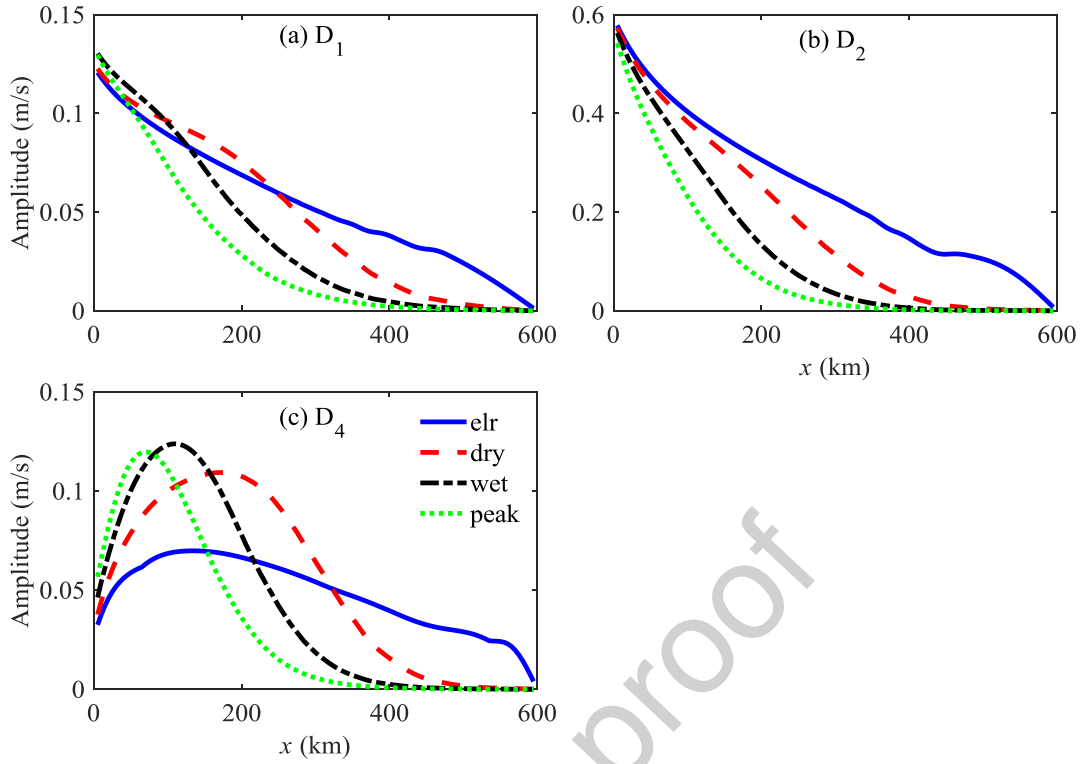

Fig. 6. Longitudinal variation in the tidal velocity amplitudes of diurnal (a), semi-diurnal (b) and quarter-diurnal tidal species (c) for the different, given river discharge conditions.

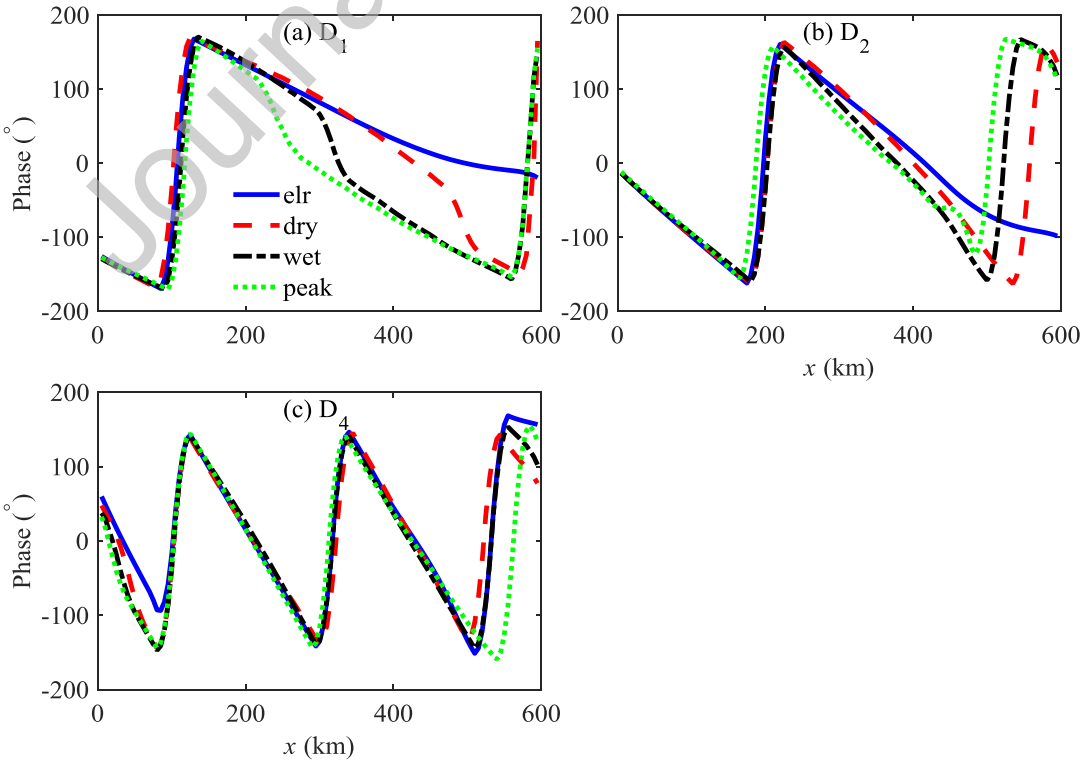

Fig. 7. Longitudinal variation in the tidal velocity phases of diurnal (a), semi-diurnal (b) and quarter-diurnal tidal species (c) for the different, given river discharge conditions.

3.7 Decomposition of the residual water level and its slope

The longitudinally varying residual water level and its slope obtained using the analytical decomposition method presented in Section 2.2 for different river discharge conditions is shown in Fig. 8. The residual water level and its slope profiles for the peak and typical wet season are considerably steeper than those during the typical dry season and elr conditions. Obviously, this is induced by the dramatic increase in freshwater, which is seasonally injected into the estuary from the catchment. Consequently, the residual water level and its slope in the upstream part (close to the Datong hydrological station) are approximately 10 m higher and 2×10^{-5} steeper during the wet season than the dry season, while the residual water level and its slope near the mouth are more or less the same during the seasonal changes in river discharges because they are mainly determined by the local mean sea level and tidal wave deformation. The tidal amplitudes decrease in the landward direction (Fig. 6), while the seasonal residual water levels decrease in the seaward direction (Fig. 8), indicating the damping effect of the residual water level on the tidal propagation and the barrier effect of the tide on the river discharge (Sassi and Hoitink, 2013; Zhang et al., 2018). The damping of the main tidal species is stronger during the wet season than during the dry season, mostly due to the higher flow velocity in the river under larger river discharges. The dynamic interplay between the tidal waves and river discharge is probably best explained in terms of the gradual adaptation of the residual water level to the changing river discharges, as discussed by Cai et al. (2016, 2018).

The analytical expression (10) can be used to explore the relative importance of river flow (f_r), tide asymmetry (f_t) and tide-river interactions (f_{tr}) on the backwater hydrodynamics. The contributions by river flow alone (f_r), tide-river interaction (f_{tr}) and tidal asymmetry (f_t) to the total residual water level under different river discharge conditions are shown in Fig. 9. The residual water level and its slope are dominated by the river discharge in the upstream parts and by the tide-river interaction at the downstream parts, which accounts for more than 90% and 80% of the total residual water level, respectively. The contribution made by tidal asymmetry is minor, accounting for less than 5% when the river discharge increased to more than 15,000 $m^3\ s^{-1}$. The contribution made by the river flow alone increased in the upstream direction and with the

increase in river discharge. In contrast, the contribution made by the tide-river interaction decreased in the upstream direction and with the increase in river discharge. The exponential decrease in the landward direction indicates the fast dissipation of tide-river interaction and its contribution to the residual water level, while the parabolic decrease in river flow contribution to the residual water level in the seaward direction indicates the fast diffusion of river flow laterally over the width at downstream of the estuary. In contrast, the tidal asymmetry produces instantaneous water level fluctuations but does not change the mean water levels.

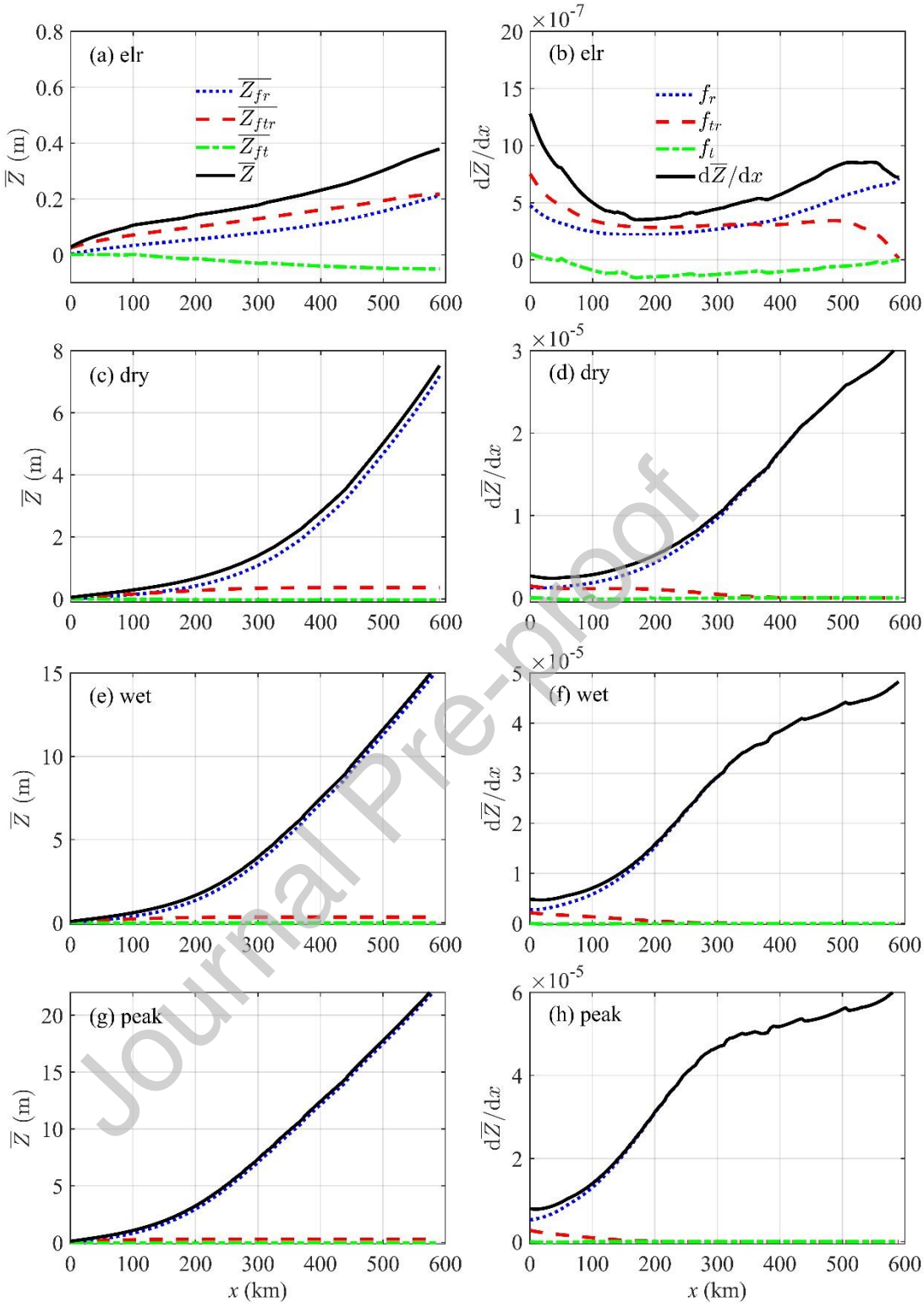

Fig. 8. Longitudinal variations in the residual water level (a, c, e, g) and its slope (b, d, f, h), where the residual water level and its slope have been decomposed into different contributions made by river flow alone, tide-river interaction and tidal asymmetry with Eq. (10). The computed results were obtained for the given river discharge conditions (a, b: elr; c, d: typical dry season; e, f:

typical wet season; and g, h: peak discharge).

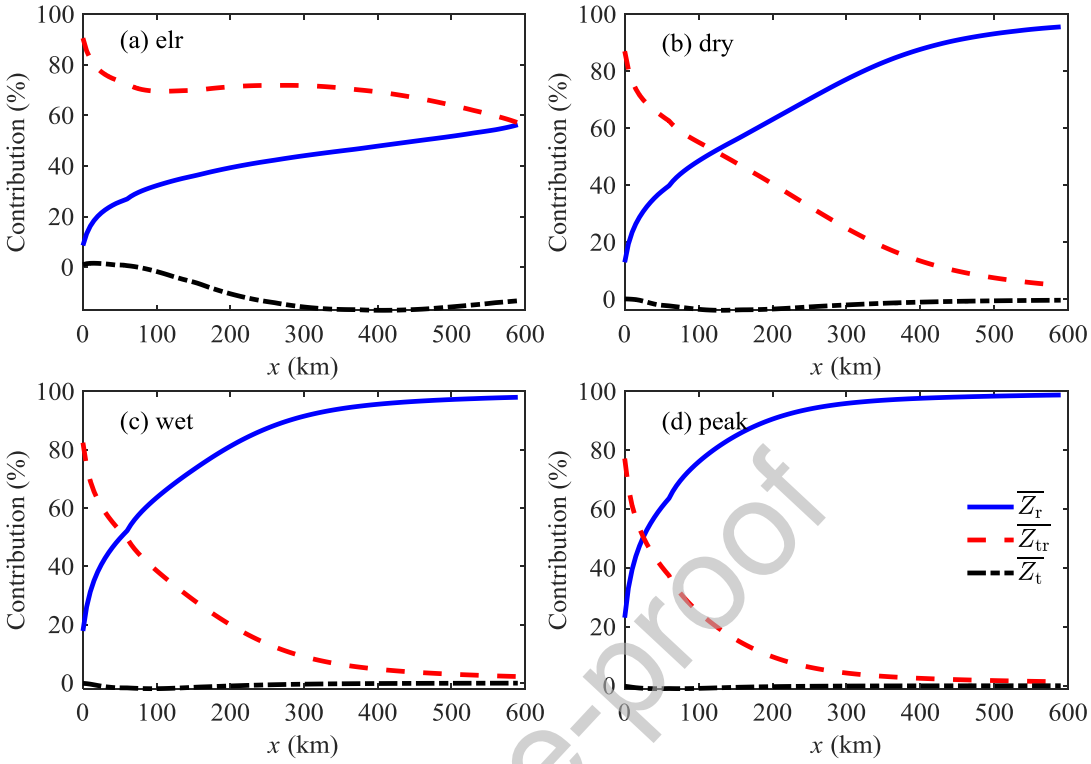

Fig. 9. Contributions to the residual water level along the channel due to river flow alone (f_r), tide-river interaction (f_{tr}) and tidal asymmetry (f_t) for different river discharge conditions: (a) elr; (b) typical dry season; (c) typical wet season; and (d) peak discharge.

4. Discussion

4.1 Contributions made by different tidal species to the residual water level

As discussed by Sassi and Hoitink (2013) and Zhang et al. (2018), tidal amplitudes decrease in the landward direction due to the damping by bottom friction and river discharge. While the residual water levels decrease in the seaward direction due to the barrier effect of the tide on the river discharge. However, the relative contributions made by different tidal species to the residual water level and its slope are not fully understood, since so far, the analyses are mostly based on the nonstationary tidal harmonic analysis (e.g., Matte et al. 2013, 2014; Guo et al., 2014, 2015). For instance, Guo et al. (2014) showed nonstationary and nonlinear tide-river dynamics along the Yangtze estuary and in the region beyond the point of tidal extinction, accounting for the contributions made by different tidal constituents. Similar nonstationary tide-river interactions have been identified in other large alluvial estuaries, such as the Amazon estuary, where the

modulation of tidal amplitudes varies with river flow in a nonlinear fashion (Kosuth et al., 2009).

To quantify the contributions made by different tidal species to the resulting residual water level owing to tide-river interactions, we decompose the residual water level component made by the tide-river interaction (see the expression of f_{tr} in Eq. 10) based on the Fourier analysis considering the 3 principle tidal species, i.e., diurnal tide (D_1), semidiurnal tide (D_2) and quarter-diurnal tide (D_4). We omit the contribution by the tidal asymmetry, as it is relatively minor when compared to the other two components (see Fig. 9). The longitudinal variations in the different contributions made to the residual water levels by diurnal, semidiurnal and quarter-diurnal tidal species were compared with the total residual water levels induced by the tide-river interaction for different river discharge conditions to derive their percentage contributions (Fig. 10). Figure 10 shows that the dominant contribution made to the residual water level is the semidiurnal tide, which accounts for approximately 70% of the total residual water level with regard to the tide-river interaction process. The diurnal and quarter-diurnal tides contributions to the residual water level are minor and comparable in magnitudes in the downstream reach within 250 km from the estuary mouth, where the contribution by the quarter-diurnal (D_4) overtide slightly increases in percentage contribution along the channel, which is likely due to the channel convergence leading to the potential energy gain from riverine flow for high river discharge conditions (Cai et al., 2018). While, the contribution made by diurnal tide (D_1) shows slight increase further upstream from 250 km, which may be due to the channel divergence (i.e., landward increase in cross-sectional area) leading to the potential energy gain from riverine flow for high river discharge conditions (Cai et al., 2018). Notably, the contribution by the diurnal tide increases and that by the quarter-diurnal (D_4) overtide decreases with the increase of river discharges. Details about the D_4 tide contribution to the residual water level are shown in Fig. S10 in the Supporting Information.

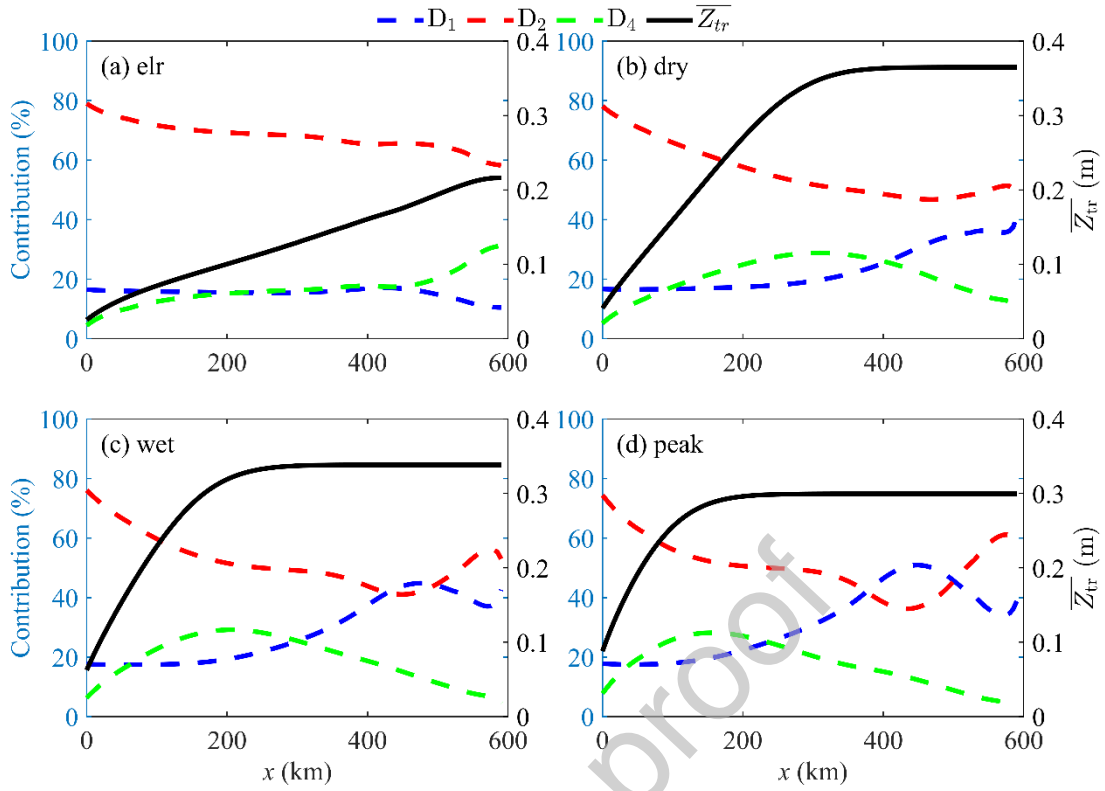

Fig. 10. Contributions made by different tidal species to the residual water level generation owing to the tide-river interaction $\overline{Z_{tr}}$ along the channel for different river discharge conditions: (a) elr; (b) typical dry season; (c) typical wet season; and (d) peak discharge.

4.2 The role of bathymetry in backwater hydrodynamics

Figure 11 shows the longitudinal variations of the numerically computed residual water level, mean water depth, cross-sectional area and its gradient for different river discharge conditions. Notably, as the residual water level increases with river discharge, the cross-sectional area also increases owing to the increasing mean water depth. Moreover, as seen from Fig. 11c, during the peak flow condition, there is a minimum value of cross-sectional area corresponding to a critical position in the upstream part of the estuary, beyond which the cross-sectional area increases slightly in the landward direction.

This results in a switch in the cross-sectional area gradient from negative (indicating a convergent cross-sectional area) to positive (indicating a divergent cross-sectional area) value. Figure 8 shows that the residual water surface slope tends to become constant in the upstream part, which is related to the river discharge influence on the backwater hydrodynamics, which on the one hand, enhances the residual frictional effect by increasing the quadratic velocity in the friction

term and reduces the channel convergence by increasing the water depth (see Fig. 11c, d), and on the other hand, reduces the effective friction by increasing the mean water depth in the numerator of the friction term (see also Cai et al. 2019).

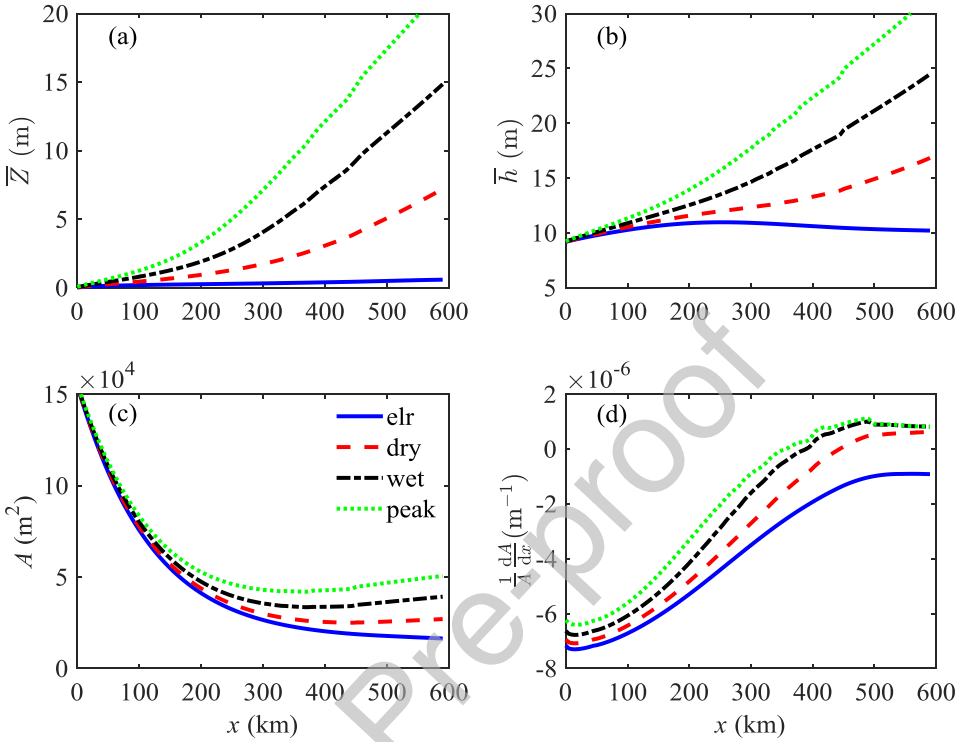

Fig. 11. Longitudinal variations in the range of residual water level $\bar{Z}$ (a), mean water depth $\bar{h}$ (b), cross-sectional area A (c), and cross-sectional area gradient dA/(Adx) in the idealized estuary.

4.3 The generation of the residual water level by other factors

This research was mainly designed to quantify the secondary and quarter-diurnal tidal species as well as the river flow (f_r), tide-river interaction (f_{tr}) and tidal asymmetry (f_t) contributions to the residual water level based on numerical simulation and analytical decomposition method of the residual water level slope. For a deeper insight, the contributions made by different tidal species to the residual water level generation owing to the tide-river interaction $\overline{Z_{tr}}$ and the role of channel convergence on backwater hydrodynamics were also discussed. However, there are still many other factors that may exert important influences on the backwater hydrodynamics. Such as in estuaries having wide intertidal area may raise residual water level through the reinforced degree of tidal distortion (Friedrichs and Aubrey, 1988); the occurrence of extreme anomalies of low-level atmospheric circulations (like Typhoon induced storm surges in west Pacific) may cause

significant changes of water levels (Escobar et al., 2004); the change of along channel salinity gradient may result in a residual water level amounting to 1.25% of the estuary depth over the salt intrusion length (Savenije, 2012); the influences of subtidal and seasonal changes of the bed roughness (Berne, 1993; Winterwerp, 2011) and the role of advective acceleration (Savenije, 2012) were all proved to have some effects on the change of residual water levels. However, they are out of the scope of this research and require further study in the future.

4.4 Improvement to the previous analytical approach

Recently, Cai et al. (2014a, 2014b, 2016, 2019) proposed an analytical approach to explore the impact of river-tide dynamics on the behavior of backwater hydrodynamics in tidal rivers. The most distinguished advantage of this analytical approach lies in that it allows for a quick prediction of tidal wave propagation with only limited data input at both ends of an estuary by solving a set of four implicit equations. However, the analytical calculation and theoretical analysis only account for one predominant tidal constituent (e.g., semidiurnal M_2 tide), which assumes negligible impacts of major secondary tidal species (e.g., D_1) and the contribution made by tidal asymmetry due to overtide generation (e.g., D_4) and their interaction between different tidal species (e.g. D_1 and D_2, D_1 and D_4, D_2 and D_4). To fill in this knowledge gap, in this contribution, an analytical decomposition method used together with a fully nonlinear 2D numerical model of TELEMAC to help understanding the impacts of the secondary tidal species and quarter-diurnal tide on backwater hydrodynamics. The novelty of this study relies on the decomposition of the quadratic velocity in the friction term, which allows for the quantification of different components (i.e., tide, river and tide-river interaction) to the generation of residual water level by Fourier decomposition into primary tidal species.

4.5 Implications for sustainable water management in tidal rivers

Tidal rivers are the transition zones between oceans and rivers, which are among the most complex areas on earth due to the substantial interactions of biological, geochemical and physical processes influenced by both rivers and oceans (Wu et al., 2012; Guo et al., 2018). By decomposing the residual water level slope into river flow alone, tide-river interaction and tidal asymmetry components and analyzing the contributions of different primary tidal species, the schematized numerical simulation designed in this study may help to understand how backwater hydrodynamics can physically control sediment transport, salinity and ecology over a range of

spatial and temporal scales.

Previous studies mainly focused on the primary tidal constituents of M_2 and its overtides M_4 on residual sediment transport and morphodynamics by analyzing the tidal asymmetry, without considering other secondary tidal species (e.g., D_1 and D_4) (Matte et al., 2013; Guo et al., 2014; 2018). They concluded that a flood tidal asymmetry tends to induce a landward residual sediment transport and therefore deposition of the riverbed, while an ebb tidal asymmetry causes a seaward residual sediment transport and therefore erosion of the riverbed (Guo et al., 2014). However, the analytical expressions derived from current contribution demonstrate that the interaction of D_2 tide with other secondary species of D_1 and D_4 will also contribute to repetitive asymmetric flow patterns. Hoitink et al. (2003) showed in their idealized study that residual sediment transport due to the tidal asymmetry induced by D_2 and D_1 tides are comparable to that of associated with the D_2 and D_4 tides. The rate of sediment transport bears a nonlinear relation with flow velocity (Hoitink et al., 2003). Therefore, flow asymmetry induced by both secondary and quarter-diurnal tidal species exerts an important influence on the degree and direction of residual sediment transport.

Moreover, the residual water level setups induced by the interactions between the tide and river flow can also have a direct effect on salinity transport. High-discharge conditions tend to generate a steep water surface profile and spatial acceleration of the ebb flow for the lower reach of estuary and therefore prevention of the saltwater intrusion, while a low residual water level during the dry season amplifies the tidal motion and promotes saltwater intrusion (Savenije et al., 2012). Besides, the variations in residual water levels can cause variations in water depth that have an impact on regional ecosystems and navigation channels (Hoitink and Jay, 2016; Nienhuis et al., 2018). In tidal rivers and riparian wetlands, the production of dissolved organic and inorganic particles, such as chlorophyll, carbon and nitrogen, varies with residual water level changes by seasonal and tidal inundation; thus, this subject deserves management attention (Hoitink et al., 2003; Leonardi et al., 2015).

5. Conclusions

In this study, we explored the impacts of secondary tidal species (D_1) and the quarter-diurnal tide (D_4) on backwater hydrodynamics in tidal rivers by means of a simplified numerical model describing the nonlinear tide-river dynamics in the Yangtze estuary. An analytical decomposition method was designed to investigate the relative contributions to the rising residual water level by

components of the river flow alone, tide-river interaction and tidal asymmetry along a tidal river for four distinct river discharge conditions, representing elr, typical dry season, typical wet season, and extremely peak discharges. Even during low river discharge conditions (i.e., elr and typical dry season), the tide-river interactions contribute remarkably to the generation of residual water level slopes. In particular, we observed that the contribution by tidal asymmetry to the residual water level is minor compared with the river flow and tide-river interaction components, which account for more than 90% and 80% at the upstream and downstream boundary, respectively. The contribution by the river flow increases in the upstream direction and with increasing river discharge. In contrast, the contribution by the tide-river interaction decreases in the upstream direction and with the increase in river discharge. Our analysis shows the dominant tidal species controlling the tidal amplitude in the Yangtze estuary is the semidiurnal tide, which accounts for approximately 70% of the residual water level caused by the tide-river interaction. The contributions by the diurnal and quarter-diurnal tidal species are minor and comparable in the seaward reach, where the tide-river interaction component is considerable. Our study assesses in detail the impacts of the different tidal constituents on tide-river dynamics, which enhances our understanding of the tidal and riverine impacts on estuarine backwater hydrodynamics and guide effective and sustainable water management (e.g., navigation, flood control, salt intrusion, etc.) in the Yangtze estuary and other tidal rivers with substantial freshwater discharge.

Acknowledgements

The research reported herein is funded by the National Key R&D of China (Grant No. 2016YFC0402600), by the National Natural Science Foundation of China (Grant No. 41476073, 51709287, 41701001 and 51979296), by the Open Research Fund of State Key Laboratory of Estuarine and Coastal Research (Grant No. SKLEC-KF201809), by the Guangdong Provincial Natural Science Foundation of China (Grant No. 2017A030310321) and by the China Postdoctoral Science Foundation (Grant No. 2018M630414).

References

Berne, B. J., 1993. Theoretical and numerical methods in rate theory. Activated Barrier Crossing, ed., Hänggi and Fleming, World Scientific, London.

Buschman, F.A., Hoitink, A.J.F., van der Vegt, M. and Hoekstra, P., 2009. Subtidal water level variation controlled by river flow and tides. Water Resources Research, 45(10): W10420.

Cai, H., Savenije, H.H.G. and Jiang, C., 2014a. Analytical approach for predicting fresh water discharge in an estuary based on tidal water level observations. Hydrology and Earth System Sciences, 18(10): 4153-4168.

Cai, H., Savenije, H.H.G. and Toffolon, M., 2014b. Linking the river to the estuary: Influence of river discharge on tidal damping. Hydrology and Earth System Sciences, 18: 287-304.

Cai, H., Savenije, H.H.G., Jiang, C., Zhao, L. and Yang, Q., 2016. Analytical approach for determining the mean water level profile in an estuary with substantial fresh water discharge. Hydrology and Earth System Sciences, 20(3): 1177-1195.

Cai, H., Yang, Q., Zhang, Z., Guo, X., Liu, F. and Ou, S., 2018. Impact of river-tide dynamics on the temporal-spatial distribution of residual water level in the Pearl River Channel Networks. Estuaries and Coasts, 41(7): 1885-1903.

Cai, H., Savenije, H. H. G., Garel, E., Zhang, X., Guo, L., Zhang, M., Liu, F. and Yang, Q., 2019. Seasonal behaviour of tidal damping and residual water level slope in the Yangtze River estuary: identifying the critical position and river discharge for maximum tidal damping, Hydrology and Earth System Sciences, 23: 1-16.

Dai, Z., Fagherazzi, S., Mei, X., Chen, J. and Meng, Y., 2016. Linking the infilling of the North Branch in the Changjiang (Yangtze) estuary to anthropogenic activities from 1958 to 2013. Marine Geology, 379: 1-12.

Dalrymple, R.W. and Choi, K., 2007. Morphologic and facies trends through the fluvial–marine transition in tide-dominated depositional systems: A schematic framework for environmental and sequence-stratigraphic interpretation. Earth-Science Reviews, 81(3-4): 135-174.

Dalrymple, R.W., Zaitlin, B.A. and Boyd, R., 1992. Estuarine facies models conceptual basis. Journal of Sedimentary Petrology, 62(6): 1130-1146.

Dronkers, J.J., 1964. Tidal computations in rivers and coastal waters. North-Holland Publishing Company, Amsterdam.

Escobar, G., Vargas, W. and Bischoff, S., 2004. Wind tides in the Rio de la Plata estuary: Meteorological conditions. International Journal of Climatology, 24(9): 1159-1169.

Friedrichs, C.T. and Aubrey, D.G., 1988. Non-linear tidal distortion in shallow well-mixed

estuaries: a synthesis. Estuarine, Coastal and Shelf Science, 27(5): 521-545.

Godin, G., 1991. Compact approximations to the bottom friction term, for the study of tides propagating in channels. Continental Shelf Research, 11(7): 579-589.

Godin, G., 1999. The propagation of tides up rivers with special considerations on the upper Saint Lawrence River. Estuarine, Coastal and Shelf Science, 48(3): 307-324.

Godin, G. and Martínez, A., 1994. Numerical experiments to investigate the effects of quadratic friction on the propagation of tides in a channel. Continental Shelf Research, 14(7−8): 723-748.

Guo, L., van der Wegen, M., Roelvink, J.A. and He, Q., 2014. The role of river flow and tidal asymmetry on 1-D estuarine morphodynamics. Journal of Geophysical Research: Earth Surface, 119(11): 2014JF003110.

Guo, L., van der Wegen, M., Jay, D.A., Matte, P., Wang, Z.B., Roelvink, D. and He, Q., 2015. River-tide dynamics: Exploration of nonstationary and nonlinear tidal behavior in the Yangtze River estuary. Journal of Geophysical Research: Oceans, 120(5): 3499-3521.

Guo, L., Brand, M., Sanders, B.F., Foufoula-Georgiou, E. and Stein, E.D., 2018. Tidal asymmetry and residual sediment transport in a short tidal basin under sea level rise. Advances in Water Resources, 121: 1-8.

Hervouet, J., 2000. TELEMAC modelling system: an overview. Hydrological Processes, 14(13): 2209-2210.

Hoitink, A.J.F., Hoekstra, P. and van Maren, D.S., 2003. Flow asymmetry associated with astronomical tides: Implications for the residual transport of sediment. Journal of Geophysical Research: Oceans, 108(C10): 3315.

Hoitink, A.J.F. and Jay, D.A., 2016. Tidal river dynamics: Implications for deltas. Reviews of Geophysics, 54(1): 240-272.

Hoitink, A.J.F., Hoekstra, P. and van Maren, D.S., 2003. Flow asymmetry associated with astronomical tides: Implications for the residual transport of sediment. Journal of Geophysical Research: Oceans, 108(C10): 3315.

Jay, D.A. and Flinchem, E.P., 1997. Interaction of fluctuating river flow with a barotropic tide: A demonstration of wavelet tidal analysis methods. Journal of Geophysical Research: Oceans, 102(C3): 5705-5720.

Jay, D.A. and Kukulka, T., 2003. Revising the paradigm of tidal analysis-the uses of non-stationary

data. Ocean Dynamics, 53(3): 110-125.

Kästner, K., Hoitink, A., Torfs, P., Deleersnijder, E., and Ningsih, N., 2019. Propagation of tides along a river with a sloping bed. Journal of Fluid Mechanics, 872, 39-73.

Kosuth, P., Callède, J., Laraque, A., Filizola, N., Guyot, J.L., Seyler, P., Fritsch, J.M. and Guimarães, V., 2009. Sea-tide effects on flows in the lower reaches of the Amazon River. Hydrological Processes, 23(22): 3141-3150.

Lamb, M.P., Nittrouer, J.A., Mohrig, D. and Shaw, J., 2012. Backwater and river plume controls on scour upstream of river mouths: Implications for fluvio-deltaic morphodynamics. Journal of Geophysical Research: Earth Surface, 117(F1): F01002.

LeBlond, P.H., 1979. Forced fortnightly tides in shallow rivers. Atmosphere-Ocean, 17(3): 253-264.

Leonardi, N., Kolker, A.S. and Fagherazzi, S., 2015. Interplay between river discharge and tides in a delta distributary. Advances in Water Resources, 80: 69-78.

Liu, J.H., Yang, S.L., Zhu, Q. and Zhang, J., 2014. Controls on suspended sediment concentration profiles in the shallow and turbid Yangtze Estuary. Continental Shelf Research, 90: 96-108.

Matte, P., Jay, D.A. and Zaron, E.D., 2013. Adaptation of classical tidal harmonic analysis to nonstationary tides, with application to river tides. Journal of Atmospheric and Oceanic Technology, 30(3): 569-589.

Matte, P., Secretan, Y. and Morin, J., 2014. Temporal and spatial variability of tidal-fluvial dynamics in the St. Lawrence fluvial estuary: An application of nonstationary tidal harmonic analysis. Journal of Geophysical Research: Oceans, 119(9): 5724-5744.

Munier, S., Litrico, X., Belaud, G. and Malaterre, P., 2008. Distributed approximation of open-channel flow routing accounting for backwater effects. Advances in Water Resources, 31(12): 1590-1602.

Nienhuis, J.H., Hoitink, A.J.F.T. and Törnqvist, T.E., 2018. Future change to tide-influenced deltas. Geophysical Research Letters, 45(8): 3499-3507.

Operating Manual, 2016. Telemac Modelling System. http://www.opentelemac.org/index.php/kunena /10-documentation (accessed 13 June 2019)

Pan, H., Lv, X., Wang, Y., Matte, P., Chen, H. and Jin, G., 2018. Exploration of tidal-fluvial interaction in the Columbia River estuary using S_TIDE. Journal of Geophysical Research: Oceans, 123(9): 6598-6619.

Parker, B.B., 1991. The relative importance of the various nonlinear mechanisms in a wide range of

tidal interactions. Wiley, J., Hoboken, N. J.

Sassi, M.G. and Hoitink, A.J.F., 2013. River flow controls on tides and tide-mean water level profiles in a tidal freshwater river. Journal of Geophysical Research: Oceans, 118(9): 4139-4151.

Savenije, H.H.G., 2012. Salinity and tides in alluvial estuaries. revised 2 Edn, https://salinityandtides.com/ (last access:17 Feburary 2020), 2012.

Savenije, H.H.G., Toffolon, M., Haas, J. and Veling, E.J.M., 2008. Analytical description of tidal dynamics in convergent estuaries. Journal of Geophysical Research: Oceans, 113(C10): C10025.

Toffolon, M., Vignoli, G. and Tubino, M., 2006. Relevant parameters and finite amplitude effects in estuarine hydrodynamics. Journal of Geophysical Research: Oceans, 111(C10): C10014.

Vignoli, G., Toffolon, M. and Tubino, M., 2003. Non-linear frictional residual effects on tide propagation, in: Proceedings of XXX IAHR Congress, Thessaloniki, Greece, vol. A, 24–29 August 2003, 291-298.

Winterwerp, J.C., 2011. Fine sediment transport by tidal asymmetry in the high-concentrated Ems River: indications for a regime shift in response to channel deepening. Ocean Dynamics, 61(2): 203-215.

Wu, J., Liu, J.T. and Wang, X., 2012. Sediment trapping of turbidity maxima in the Changjiang Estuary. Marine Geology, 303-306: 14-25.

Zhang, F., Sun, J., Lin, B. and Huang, G., 2018. Seasonal hydrodynamic interactions between tidal waves and river flows in the Yangtze Estuary. Journal of Marine Systems, 186: 17-28.

Zhang, M., Townend, I., Zhou, Y. and Cai, H., 2016a. Seasonal variation of river and tide energy in the Yangtze estuary, China. Earth Surface Processes and Landforms, 41(1): 98-116.

Zhang, M., Townend, I.H., Cai, H. and Zhou, Y., 2016b. Seasonal variation of tidal prism and energy in the Changjiang River estuary:a numerical study. Chinese Journal of Oceanology and Limnology, (01): 219-230.

Zhang, W., Cao, Y., Zhu, Y., Zheng, J., Ji, X., Xu, Y., Wu, Y. and Hoitink, A.J.F., 2018. Unravelling the causes of tidal asymmetry in deltas. Journal of Hydrology, 564: 588-604.

Zhou, Z., Coco, G., Townend, I., Gong, Z., Wang, Z.B. and Zhang, C.K., 2018. On the stability relationships between tidal asymmetry and morphologies of tidal basins and estuaries. Earth Surface Processes and Landforms, 9(43): 1943-1959.

Author statement

The authors all agree to submit the paper and publish on the journal of Advances in Water Resources if the manuscript is accepted.

Declaration of interests

☒ The authors declare that they have no known competing financial interests or personal relationships that could have appeared to influence the work reported in this paper.

☐The authors declare the following financial interests/personal relationships which may be considered as potential competing interests: